Cell Reports, Volume *42*

Supplemental information

Splicing quality control mediated by DHX15 and its G-patch activator SUGP1

Qing Feng, Keegan Krick, Jennifer Chu, and Christopher B. Burge

Figure S1

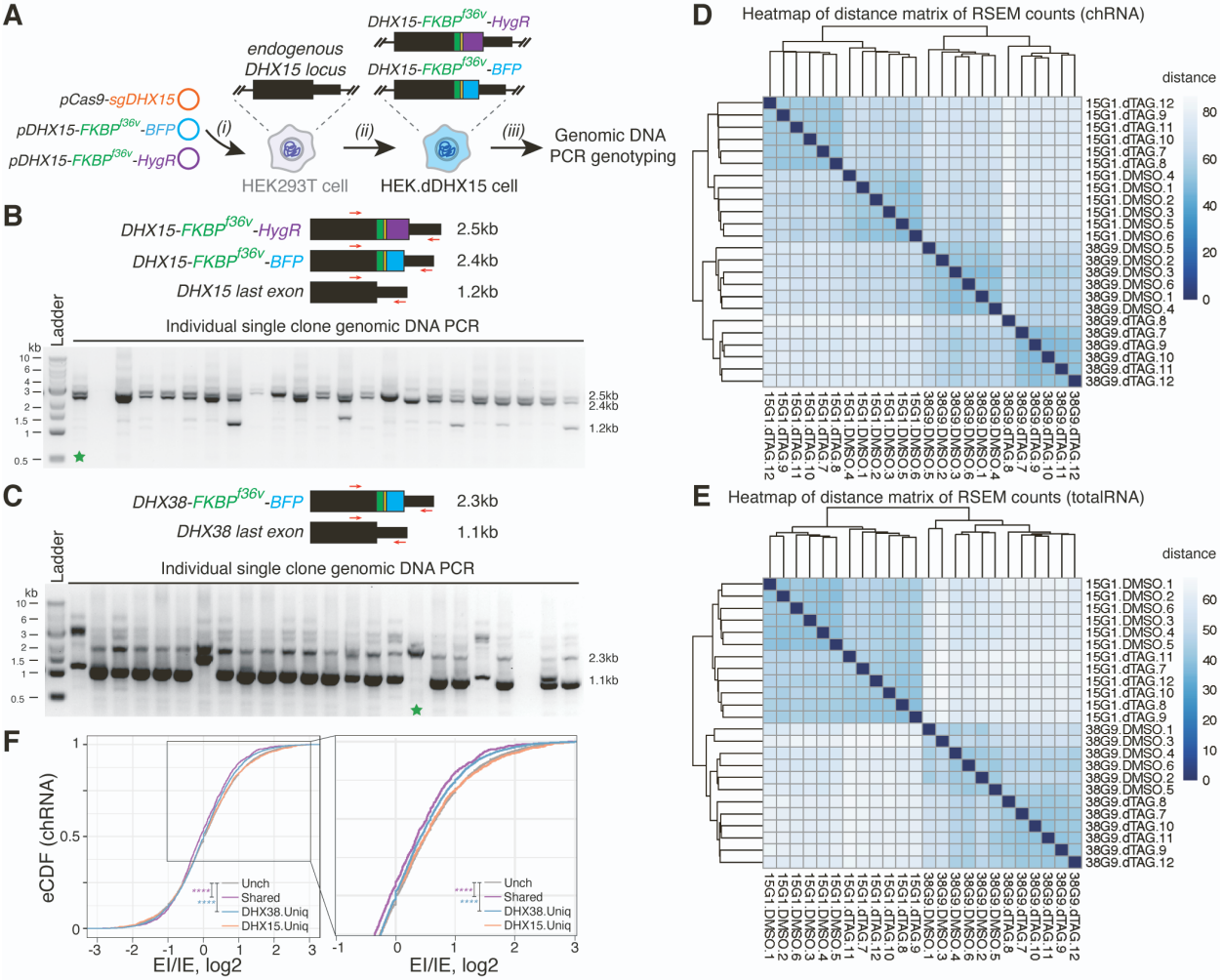

Figure S1. Cell line construction, genotyping, and RNA-seq replicate clustering, Related to Figures 1 and 2.

(A) Schematic of HEK.dDHX15 cell line construction: (i) co-transfection of gene-specific gRNA-containing pCas9 plasmid, and DNA repair template plasmids containing BFP and HygR selection markers; (ii) selection for BFP-positive and hygromycin-resistant single clones; (iii) genomic DNA extraction and genotyping. **(B)** Genotyping PCR primer design and PCR gel for HEK.dDHX15 cell line. Green star, homozygous clone (#15G1), which was later validated by Western blot (Fig. 1C) and further expanded for RNA-seq experiments. **(C)** Similar to (B), for HEK.dDHX38 cell line. Green star, homozygous clone (#38G9), which was later validated by Western blot (Fig. 2B) and further expanded for RNA-seq experiments. **(D, E)** Heatmap clustering of distance matrix of RSEM counts in the chRNA (D) and totalRNA (E) sequencing experiments with HEK.dDHX15 (#15G1) and HEK.dDHX38 (#38G9) cells. Six replicates of each condition (DMSO versus dTAG) cluster together in both chRNA and totalRNA sets.**(F)** Empirical distribution function (eCDF) of log2 ratio between exon-intron junction reads and intron-exon junction reads. Purple, shared introns with decreased splicing efficiency. Blue/Orange, DHX38/DHX15 unique substrate introns with decreased splicing efficiency. Grey (Unch), introns exhibit insignificant or unaltered changes in *SI*. Only constitutive introns are assayed here. Statistical significance is calculated by Welch's *t*-test, indicated by asterisks (****, P-value < 0.0001), unless otherwise indicated.

Figure S2

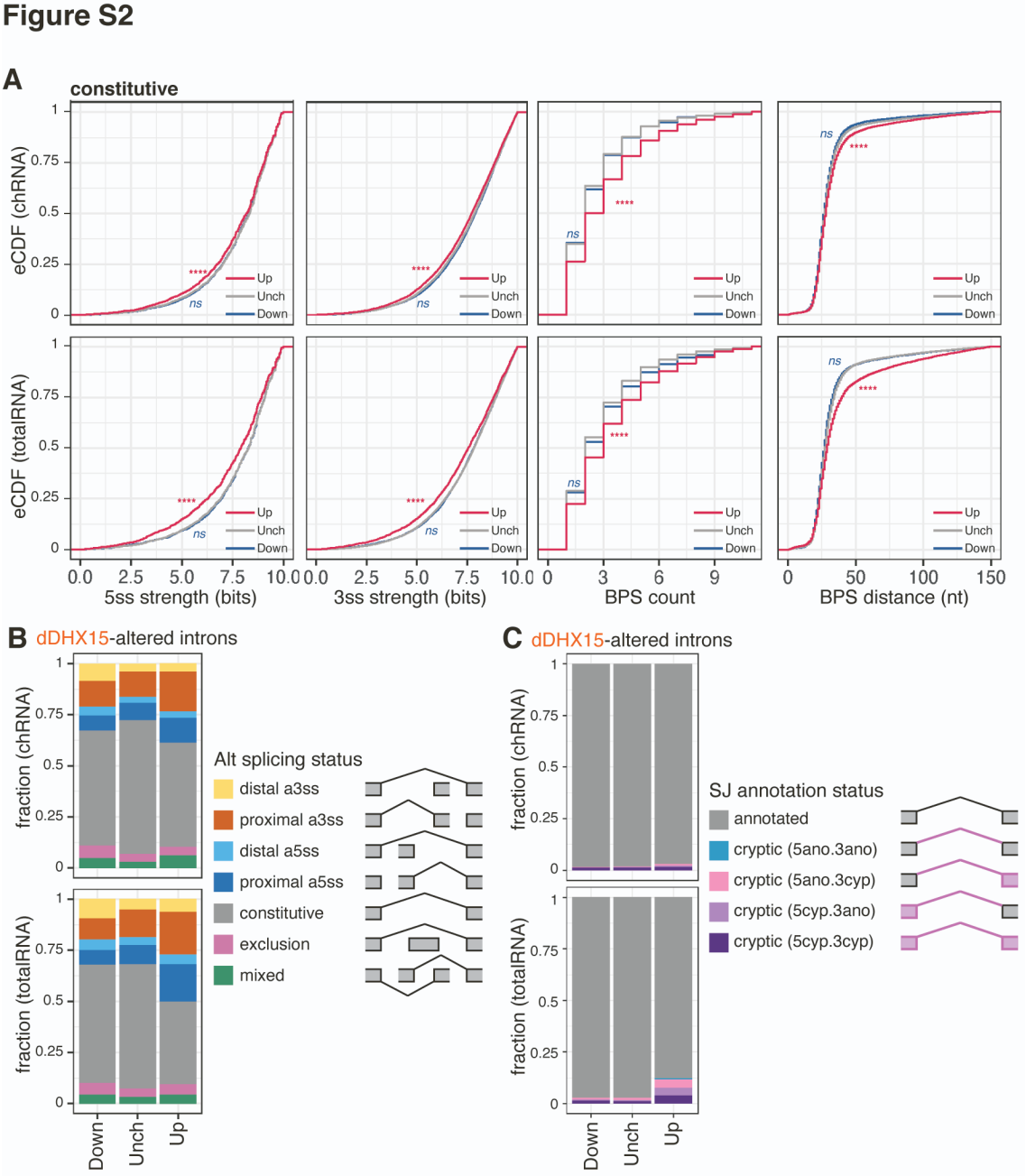

Figure S2. DHX15 represses the splicing of suboptimal constitutive, alternative and cryptic introns, Related to Figure 3.

(A) Similar to Figure 3A-C, restrict to constitutive introns. Distribution of splice sites strength MaxEntScan scores, counts of BPS per intron, and distances between BPS and 3ss for each BPS-3ss pair. Magenta/Navy (Up/Down), introns exhibiting significant (FDR ≤ 0.05) increases/decreases of *SI* ≥ 0.05, upon dTAG13-induced DHX15 depletion in HEK.dDHX15 cells. Grey (Unch), introns exhibit insignificant or unaltered changes in *SI*. 5ss, 5' splice site. 3ss, 3' splice site. Statistical significance in (A-C) is calculated by Welch's *t*-test, indicated by asterisks (****, P-value < 0.0001, ns = not significant), unless otherwise indicated. **(D)** Percentage stacked bar of constitute *v.s.* alternative splicing junctions. **(E)** Percentage stacked bar of annotated versus cryptic splicing junctions.

Figure S3

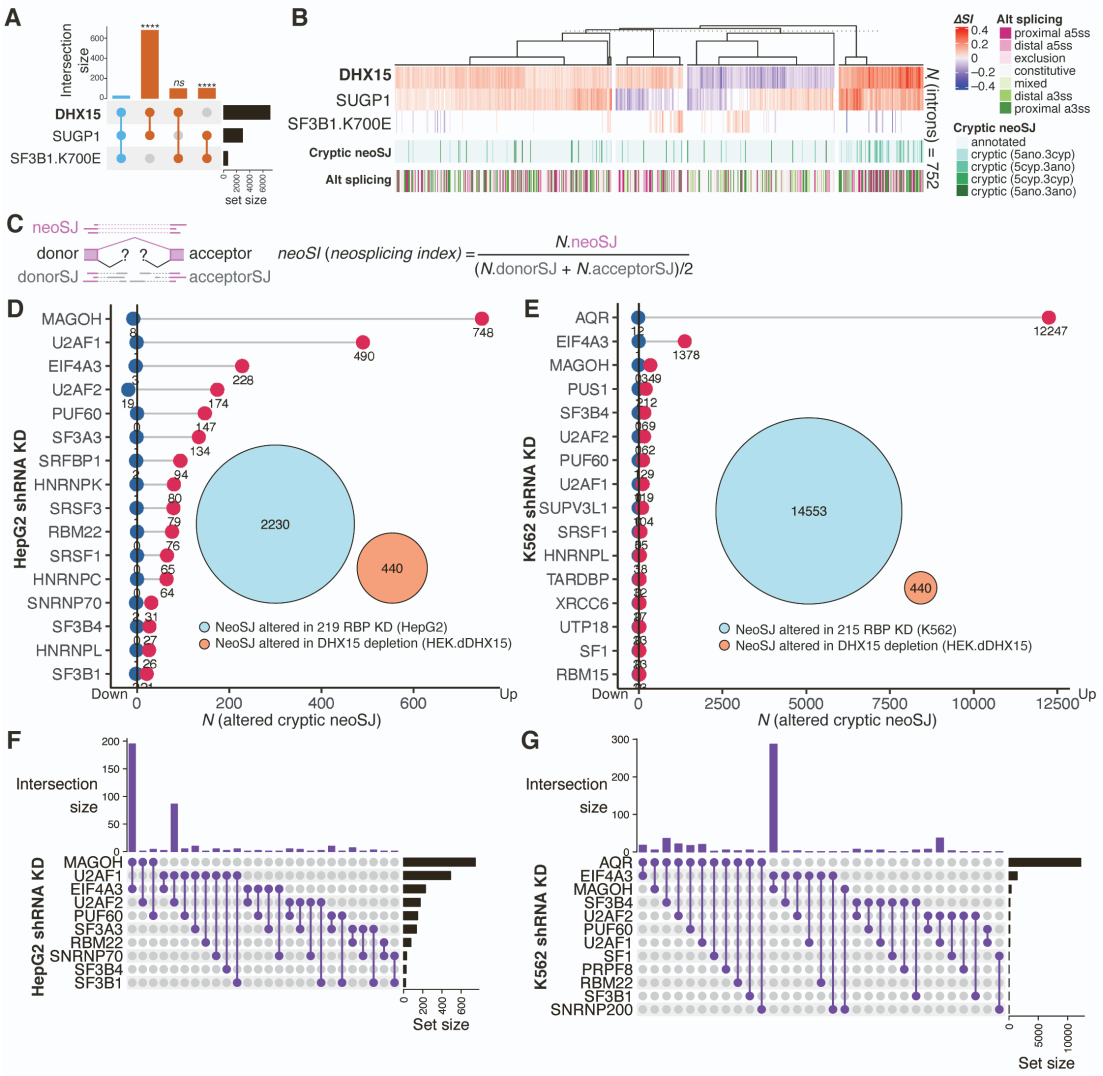

Figure S3. Cryptic neojunction splicing upon depletion of DHX15, SF3B1.K700E expression, and over 200 RBP knockdown experiments, Related to Figure 4.

(A) Intersection UpSet plot of altered introns ($|\Delta SI| \geq 0.05$, FDR ≤ 0.05) upon depletion of DHX15, KD of SUGP1, and SF3B1.K700E expression. Statistical significance of the intersection is calculated by Hypergeometric test in R (****, P-value < 0.0001; ns, not significant, P-value > 0.01). **(B)** Heatmap and hierarchical clustering of 752 introns with altered splicing efficiency ($|\Delta SI| \geq 0.05$, FDR ≤ 0.05) upon depletion of DHX15 that are also altered in either the SUGP1 KD experiment or the SF3B1.K700E experiment. **(C)** Illustration of how *neoSI (neo-Splicing Index)* is computed by taking the ratio between spliced neojunction reads and normalized total counts of spliced reads across either the donor or the acceptor of the neojunction. **(D, E)** The number of neojunctions (neoSJ) with altered *neoSI* upon knockdown of corresponding RBPs in ENCODE HepG2 (D) and K562 (E) shRNA sets. Magenta/Navy (Up/Down), counts of neoSJ exhibiting significant changes in splicing ($|\Delta neoSI| \geq 0.05$, FDR ≤ 0.05). RBP KD resulting in more than 20 altered neoSJ are shown. Inset, venn diagram showing no shared altered neoSJ upon DHX15 depletion and KD of any of the 219 RBPs in HepG2 (D, inset) and 215 RBPs in K562 (E, inset) cells. **(F, G)** Intersection UpSet plot of altered neoSJ ($|\Delta neoSI| \geq 0.05$, FDR ≤ 0.05) upon KD of spliceosomal RBPs in the HepG2 (F) and K562 (G) cells.

Figure S4

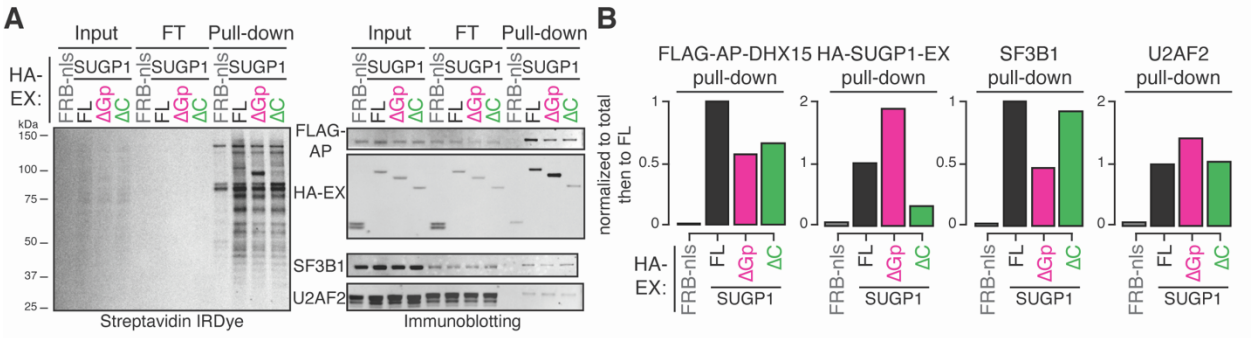

Figure S4. Assessment of SUGP1 ΔGp and ΔC interaction with DHX15, Related to Figure 6.
(A) Protein blots of biotinylated proteins labeled by full-length (FL) versus truncated SUGP1-DHX15 interaction reconstituted split-APEX activity, enriched by streptavidin pull-down experiments. ΔGp, G-patch domain truncation. ΔC, C-terminus truncation. **(B)** Quantification of pull-downs in (A).